Separation of an Inertial Boundary Current from a Curved Coastline*

HSIEN WANG OU

Lamont-Doherty Geological Observatory of Columbia University, Palisades, NY 10964

WILHELMUS P. M. DE RUIJTER

Rijkswaterstaat/Deltaservice, Van Alkemadelaan 400, 2597 AT Den Haag, The Netherlands

(Manuscript received 11 March 1985, in final form 29 August 1985)

ABSTRACT

A two-layer model is used to examine the separation of an inertial boundary current from a curved coastline and its subsequent path as a free jet. To isolate the inertial effect, the boundary current is confined to the upper layer and insulated from the ocean interior by a free streamline. The separation occurs when the interface outcrops and forms a free streamline. Besides the constraint imposed by the coastal boundary, the primary dimensionless parameter that regulates the separation point and the subsequent current path is the scaled volume flux of the current (Q). Increasing Q causes the current to separate at a lower latitude. The separation also occurs where the coastline has a large positive curvature (i.e., convex outward). After the separation, the current can either meander or loop back on itself depending on the flow direction at the separation point. Application of the model to the Agulhas Current can reproduce the retroflection feature (i.e., a current turning back on itself) with roughly the correct dimensions, suggesting that the inertial and beta effect play a dominant role in the phenomenon.

1. Introduction

This study is motivated by the observed path of the Agulhas Current, which makes an abrupt "aboutface" turn (within a few degrees latitude) after it leaves the African continent (Fig. 1, adapted from Gordon et al., 1986). As resembling the bending backward on itself of a mammalian gut, the feature has been termed "retroflection," and has intrigued many oceanographers ever since it was first documented over a century ago (Lutjeharms, 1980). Despite the enormous data assembled in recent years that describe the areal circulation in ever greater detail, the theoretical explanations of the phenomenon have largely been sketchy and not wholly satisfactory.

Assuming that the current extends to the ocean bottom, Darbyshire (1972) and Lutjeharms and Van Ballegooyen (1984) used Warren's theory (1963, slightly modified by Robinson and Niiler, 1967) to calculate the current path. The calculated path, however, varies greatly with small changes in the bottom velocity, seemingly at odds with the more persistent circulation pattern observed. Since the Agulhas Current is highly baroclinic with more than eighty percent of the mass transport concentrated within the top thousand meters of the water column (Gründlingh, 1980) and since there is no substantial topographic feature in the retroflection area, it is doubtful that the current path is mainly steered by topography. Using boundary layer analysis, De Ruijter (1982) deduced that retroflection must occur in order for the Agulhas Current to merge into the large-scale circulation of the ocean interior. His model does not, however, address the local dynamical balance of the retroflection and hence does not fully answer the questions as to why and how the current turns. Numerical calculations, such as the ones by De Ruijter and Boudra (1985) or Holland (personal communication, 1985), are able to reproduce some aspects of the retroflection but, with all the complicating elements included in the models, it is difficult to isolate the essential physical mechanisms that account for the phenomenon.

A related problem that has attracted much attention in the last two decades is the separation of the Gulf Stream from the continental slope near Cape Hatteras and its subsequent meandering path. In fact, it is the desire to explain the Gulf Stream path that motivated Warren's work in 1963. But despite considerable refinements made over the years (Robinson and Niiler, 1967; Robinson et al., 1975), whether the theory provides an adequate account of the Gulf Stream path remains a subject of much debate. While recent observations (Luyten, 1977) have cast doubts about treating the Gulf Stream as a vertically coherent flow that extends to the ocean bottom, it is quite definite that the Western Boundary Undercurrent crosses the stream axis near Cape Hatteras where the separation

* Lamont-Doherty Geological Observatory contribution Number 3914.

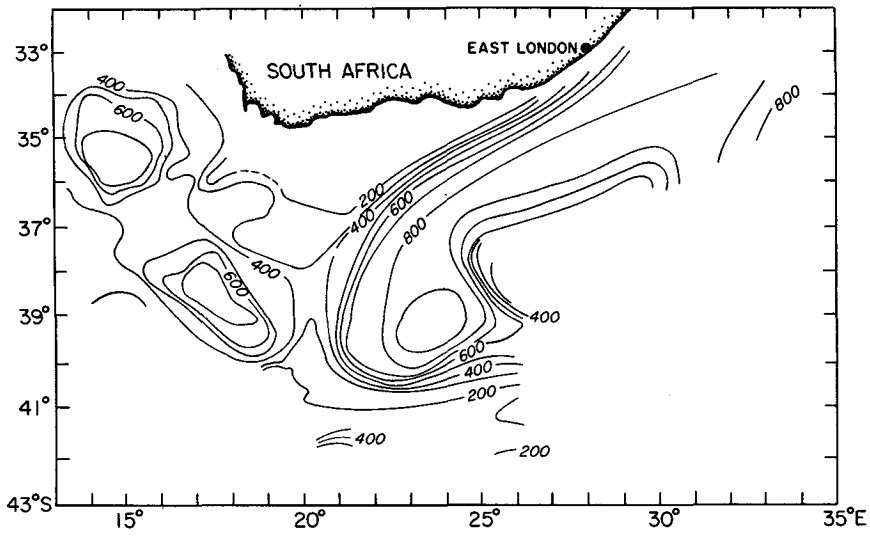

FIG. 1. Depth (in meters) of the 10°C isotherm (adapted from Gordon et al., 1986).

takes place and where the bottom flow is nearly opposite to the surface flow (Richardson and Knauss, 1971).

To exclude the topographic effect, a rather contrasting view of the Gulf Stream separation was provided by Parsons (1969) and Veronis (1973) in their reduced gravity models. In these models, the separation occurs where the interface outcrops and forms a free streamline. Since these models are essentially linear, the current path defined by the free streamline is directly related to the global wind field. There is no doubt that the basin-wide circulation plays some role in the separation of the boundary current, which after all is produced by the large scale wind field and ultimately has to merge into the ocean interior. It is unrealistic, however, to assume that for a boundary current of such enormous inertia, its path is completely determined by the far field.

Reduced gravity models have also been used by Moore and Niiler (1974) and Anderson and Moore (1979) to examine the separation problem, but one notable element that is missing in all these studies is the coastline curvature. It is perhaps not coincidental that many major boundary currents separate at coastline irregularities; besides the separation of the Agulhas Current at the southern terminus of the African continent and the Gulf Stream at Cape Hatteras, other prominent examples include the Kuroshio at Cape Inubozaki and the Eastern Australian Current near Sugarloaf Point. Intuitively, one would not expect a swift current to go around sharp corners, but the precise physical mechanism of the separation needs to be stated in more definite terms.

We shall thus consider a reduced gravity model that incorporates as essential elements the current inertia, beta effect and coastline curvature to examine the local dynamics near the separation point. The model formulation and results are presented in sections 2 through 6. The application to the Agulhas Current is presented in Section 7 followed by some discussions in Section 8.

2. The model

Let us consider a two-layer ocean bounded by a vertical wall as schematically shown in Fig. 2. For the convenience of discussions, we have positioned ourselves in the Northern Hemisphere so that the x- and y-axis are pointing east and north respectively. A western boundary current flowing north is confined to the upper layer overlying a motionless lower layer and insulated from the ocean interior by a free streamline along which the pressure and hence the interface depth is constant (denoted by H). The free streamline can be justified by assuming either that the flow there is sufficiently weak so that geostrophy holds or—more rigorously but also more restricted—that the ocean interior is at rest. For simplicity, the upstream point $y = 0$ is chosen where the coast is straight. In this two-layer configuration, the separation occurs when the interface outcrops and forms a free streamline, and the main objective of the model is to determine the upstream control of the separation point and the subsequent path of the free jet.

The jet is assumed to be sufficiently narrow that it can be conveniently described by a curvilinear system affixed to the left boundary of the jet (facing downstream). For simplicity, the governing equations are expressed in terms of nondimensionalized variables. We have scaled the Coriolis parameter f by its upstream value f_0 (the subscript "0" will be used throughout the paper to indicate the upstream value at $y = 0$), the

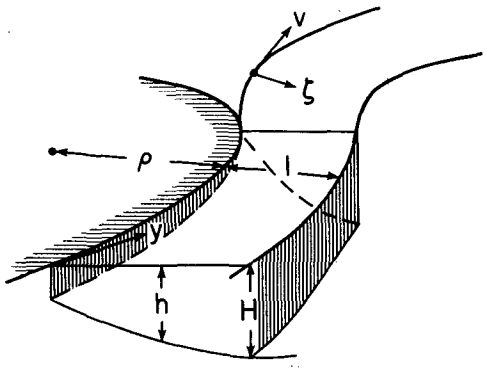

FIG. 2. Model configuration.

upper layer depth by H, the length by the internal radius of deformation λ (defined by $\sqrt{g'H}/f_0$ where g' is the reduced gravity), the velocity by $f_0\lambda$, and the volume flux by $f_0\lambda^2 H$.

Let ζ be the cross-stream coordinate and v be the alongstream velocity, a transport streamfunction ψ can be defined by

$$hv = \frac{\partial \psi}{\partial \zeta}, \tag{2.1}$$

with the values that

$$\psi = 0 \quad \text{at} \quad \zeta = 0, \tag{2.2}$$

$$\psi = Q \quad \text{at} \quad \zeta = l, \tag{2.3}$$

where Q is the volume transport and l is the jet width, an unknown function of y.

Assuming that the ocean is Boussinesq, hydrostatic and inviscid, and that the variation alongstream occurs on a scale large compared to that across-stream, the cross-stream momentum balance is governed by the equation (e.g., see Røed, 1980)

$$fv + \frac{v^2}{\rho + \zeta} = \frac{\partial h}{\partial \zeta}. \tag{2.4}$$

The scaled Coriolis parameter f, under the beta-plane approximation, is given by

$$f = 1 + \beta y, \tag{2.5}$$

where the dimensionless parameter β is defined as

$$\beta \equiv \lambda \cot\Theta_0 / R, \tag{2.6}$$

with Θ_0 being the latitude at $y = 0$ and R, the earth's radius. In (2.4), ρ is the local radius of curvature measured along the left boundary of the jet (facing downstream). The sign convention adopted here is that ρ is positive if the jet is cyclonically curved. Since for a nonseparated jet, ρ also gives the radius of curvature of the coastline, a convex (concave) coastline thus has a positive (negative) curvature.

For an inviscid fluid, the potential vorticity is conserved along streamlines and hence given by its upstream value. For simplicity, the potential vorticity will be assumed constant at $y = 0$ with the value f_0/H (i.e., the relative vorticity vanishes at the free streamline bordering the ocean interior), the conservation law thus reduces to the statement that

$$f + \frac{\partial v}{\partial \zeta} + \frac{v}{\rho + \zeta} = h. \tag{2.7}$$

Another useful conservation law is the Bernoulli's principle which states that the Bernoulli function B, defined by

$$B \equiv \frac{1}{2} v^2 + h, \tag{2.8}$$

is conserved along streamlines. From (2.4) and (2.7), it can be derived that

$$\frac{\partial B}{\partial \zeta} = hv, \tag{2.9}$$

or, upon integration,

$$[B]_0^l = Q. \tag{2.10}$$

The equations (2.4) and (2.7) form a closed system for the two dependent variables h and v. The boundary conditions are

$$h = 1 \quad \text{at} \quad \zeta = l, \tag{2.11}$$

and, through Bernoulli's principle,

$$v = v_R \text{ (a constant)} \quad \text{at} \quad \zeta = l. \tag{2.12}$$

In our terminology, the subscripts "L" and "R" are used to indicate values at, respectively, the left and right boundary of the jet facing downstream. Since the jet width is an unknown function of y, an additional constraint is needed to close the problem, which is provided by (2.3) or, equivalently, (2.10).

For given external parameters Q and v_R, the solution can be obtained numerically in the parameter space of (f, κ) where $\kappa \equiv 1/\rho$ is the local curvature. The numerical procedure goes as follows: We guess a value of l, and integrate the equations (2.4) and (2.7) cross-stream from $\zeta = l$ to $\zeta = 0$ using the boundary conditions (2.11) and (2.12). After we have reached the boundary $\zeta = 0$, the boundary constraint (2.10) is checked. The above procedure is repeated using different values of l until this boundary constraint is satisfied. Before we present the solution, we will first discuss the external parameters Q and v_R.

3. The upstream condition

The external parameters Q and v_R can be related to other flow parameters that characterize the upstream condition. Solving the problem at $y = 0$ where the coast is straight, we arrive at the expressions (see Appendix A),

$$Q = \frac{1}{2}(1 - h_{L0}^2), \tag{3.1}$$

$$v_R = (1 - h_{L0})/\sinh(l_0), \tag{3.2}$$

where h_{L0} is the interface depth at the coast and l_0 is the jet width. Both of these variables can in principle be estimated from hydrographic observations.

It is noted that Q is a function of h_{L0} only, which is plotted in Fig. 3. It has a maximum value of ½ when the interface outcrops and decreases for increasing h_{L0} until the interface becomes level and the boundary current ceases to exist. We have also plotted in Fig. 4 values of v_R as a function of h_{L0} and l_0. Since l_0 defines the jet boundary, it should be chosen where the flow is sufficiently weak. Judging from the figure, $l_0 = 3$ is a reasonable choice, a value above which v_R is negligible and the solution is not expected to be sensitive to the variation of l_0.

We thus conclude that the crucial external parameter is h_{L0}—and hence the volume transport—and that the solution is not expected to be sensitive to l_0 so long as it is greater than 3.

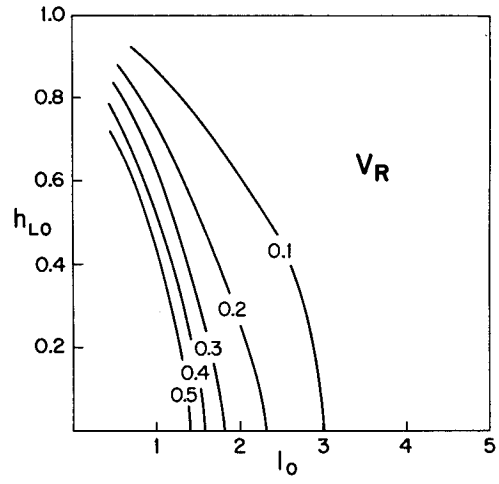

FIG. 4. Values of v_R as a function of h_{L0} and the upstream jet width l_0.

4. The separation curve

As an example of the solution, we have plotted in Fig. 5 in thin solid lines the contours of h_L (the interface depth at the coast) in the (f, κ) space for the case of $h_{L0} = 0.27$ and $l_0 = 3$. Solution exists only in the stippled area to the left of the thick solid curve (the separation curve) marking the interface outcropping. The separation curve thus gives the critical curvature of the coastline when the separation occurs or, if the flow is already separated, the curvature of the free jet. In the figure, we have also drawn a schematic curve representing a coastline and arrows indicating the flow path; the flow moves north along the coast until it intersects the separation curve upon which it becomes a free jet and moves along the separation curve. Since, given an initial flow direction, a flow path in the (f, κ) space may be uniquely translated to that in the physical space (see the next section), the specification of the separation curve is the main task of this study.

Denoting by f_c the intersection of the separation curve with the f-axis, then it represents the separation point when the coast is straight or, if the flow is already separated, an inflection point in its path. Because of the negative slope of the separation curve, the separation occurs at a lower latitude when the coast has a

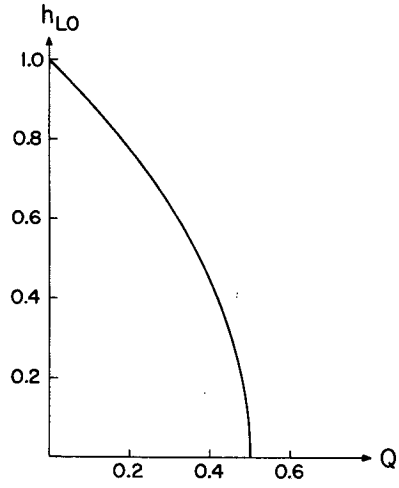

FIG. 3. Volume transport Q as a function of h_{L0} (the interface depth at coast at $y = 0$).

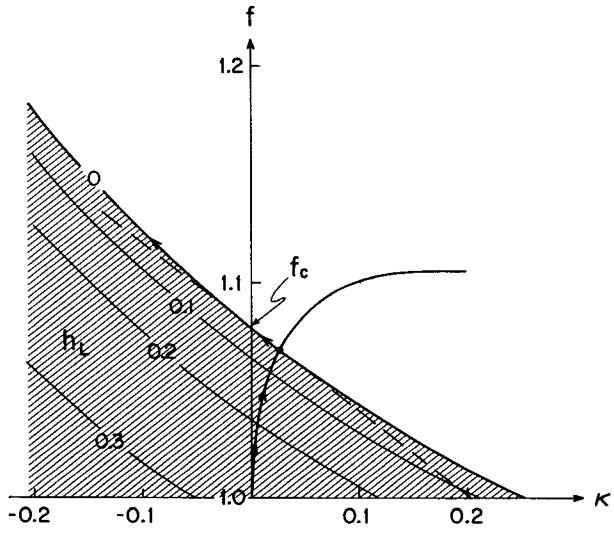

FIG. 5. Contours of h_L (the interface depth at coast, in thin solid lines) on the (f, κ) plane for the case of $h_{L0} = 0.27$ and $l_0 = 3$. Separation curve and a schematic coastline are shown in thick solid lines. The arrows indicate the flow path. The dashed line is tangent to the separation curve at f_c.

convex curvature. One trivial result is then that the flow always separates before it becomes straight (the inflection point) if the coastline curves convexly.

In a very crude sense, the separation can be explained by the following arguments: Let us first consider a jet moving poleward along a straight coast, the beta effect increases the anticyclonic shear of the current and hence a speedier flow near the coast. Geostrophy then steepens the cross-stream tilt of the interface and leads eventually to its surfacing at some poleward latitude. When the coastline has a positive curvature (i.e., convex outward), it on the one hand reinforces the beta effect in sharpening the anticyclonic shear of the current through the vorticity balance and, on the other, induces a centrifugal force, both of which tend to further steepen the interface tilt and hence a separation at a lower latitude.

Although the separation curve is slightly curved, for practical purposes, it can be approximated by its tangent at f_c, shown by the dashed line in Fig. 5. To determine f_c and the slope of this tangent, we multiply the cross-stream momentum equation (2.4) by h and integrate across the stream to yield, along the separation curve,

$$fQ + \int_0^l \frac{hv^2}{\rho + \zeta}\, d\zeta = \frac{1}{2}. \tag{4.1}$$

Evaluation of the above expression at f_c, where ρ is infinite, leads to

$$f_c = \frac{1}{2Q}. \tag{4.2}$$

Thus f_c is a function of Q only and the dependence is reciprocal. Physically, a greater transport implies a shallower interface at the coast and hence separation at a lower latitude.

If we vary (4.1) along the separation curve and then evaluate it at f_c, we obtain

$$Q\delta f + M_c\delta\kappa = 0, \tag{4.3}$$

where $M_c \equiv \int_0^l hv^2 d\zeta$ is the momentum transport at f_c. Let α denote the slope of the separation curve at f_c, then

$$\alpha \equiv \frac{\delta\kappa}{\delta f} = -\frac{Q}{M_c}. \tag{4.4}$$

Since the curvature is zero at f_c, an analytical expression can be derived for M_c and hence α (see Appendix B) which are plotted in Figs. 6 and 7. As expected from discussions in Section 3, for l_0 greater than 3, the slope of the separation curve is essentially a constant in l_0, but, additionally, it varies only slowly with h_{L0} except when h_{L0} is very near unity (i.e., a vanishing flow). Because the momentum transport varies with h_{L0} at a slower rate than the volume transport (compare Figs. 3 and 6), the separation curve steepens slightly with decreasing h_{L0} (or increasing volume transport). We thus conclude that the separation curve is basically a

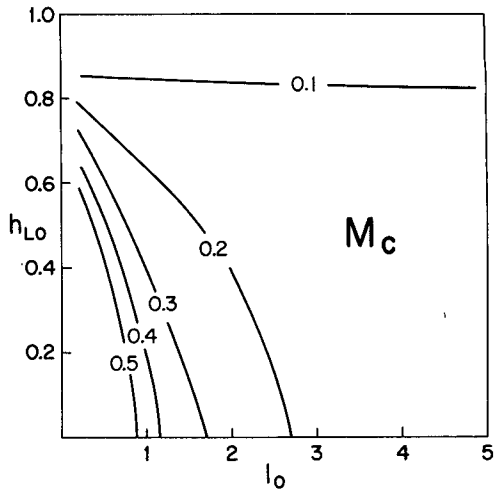

FIG. 6. As in Fig. 4 but for M_c, the momentum transport at f_c.

function of the volume transport and the dependence is mainly through changes in f_c.

5. The jet path

From the sketch shown in Fig. 8, we observe that

$$\rho d\vartheta = -\frac{dy}{\cos\vartheta}, \tag{5.1}$$

where ϑ gives the flow direction, measured clockwisely from north. By rearranging and integrating the above equation, one obtains

$$-[\sin\vartheta] = \frac{1}{\beta}\int \kappa df. \tag{5.2}$$

For a prescribed $\kappa(f)$ and an initial flow direction, the formula allows us to calculate the subsequent flow direction as a function of the latitude and hence the flow path in the physical space. In referring to Fig. 5, the term on the right-hand side of (5.2) is proportional to the area straddled between the f-axis and the flow path indicated by the arrows. Since the left-hand side has an upper bound given by $1 + \sin\vartheta_0$ (i.e., when the flow becomes due west), the flow may or may not reach f_c. In the latter case, the flow simply traces back along the separation curve until it is again constrained by the coastal boundary, while in the former case, the flow begins to curve anticyclonically and, depending on the current direction at the inflection point, can follow quite different paths.

To examine this, we set $\kappa = \alpha(f - f_c)$ in (5.2) to arrive at

$$\sin\vartheta = \sin\vartheta_c - \frac{\alpha\beta}{2}(y - y_c)^2, \tag{5.3}$$

where the subscript "c" refers to the values at the inflection point f_c. Substituting (5.3) into the expression

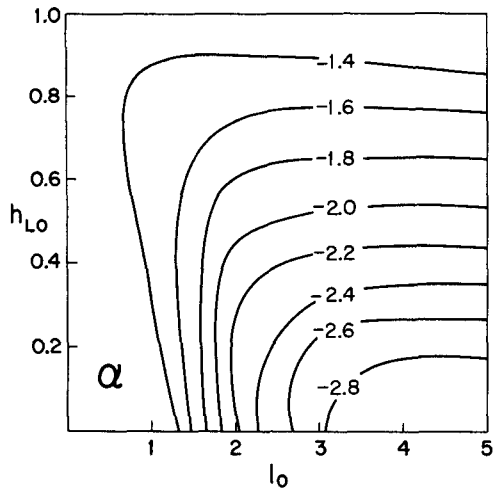

FIG. 7. As in Fig. 4 but for α, the slope of the separation curve at f_c.

$$\frac{dx}{dy} = \tan\vartheta = \sin\vartheta(1 - \sin^2\vartheta)^{-1/2}, \qquad (5.4)$$

and integrate, the flow path can be calculated numerically, a few examples of which, corresponding to different values of ϑ_c, are shown in Fig. 9. It is seen that the flow can either double back on itself, thus forming closed loop, or meander back and forth as it streams eastward.

To determine the turning latitude where the flow becomes eastward, we set ϑ to $\pi/2$ in (5.3) to yield

$$\left(\frac{-\alpha\beta}{2}\right)^{1/2}(y - y_c) = (1 - \sin\vartheta_c)^{1/2}, \qquad (5.5)$$

which is plotted in Fig. 10. The turning latitude thus is a decreasing function of ϑ_c and has a bounded maximum when the flow is nearly due west at the inflection point. Dimensionally, this maximum value, which is $\sqrt{2}$ for the expression (5.5), corresponds to a turning latitude (measured from the inflection point) of

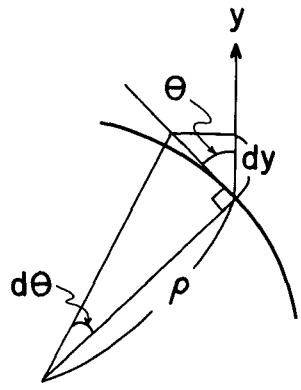

FIG. 8. A schematic that relates curvature to the flow direction (measured clockwise from north).

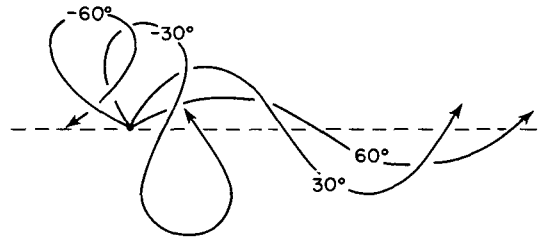

FIG. 9. Current paths for different values of ϑ_c, the flow direction at the inflection point.

$$\Delta\Theta \equiv \lambda(y - y_c)/R = 2\left(\frac{\lambda \tan\Theta_0}{-\alpha R}\right)^{1/2}, \quad \text{(using Eq. 2.6)} \qquad (5.6)$$

It is interesting to note from (5.6) that the penetration distance from the inflection point decreases for greater volume transport (hence α) or smaller internal radius of deformation.

To calculate the meandering wavelength, we first notice that the first integral of (5.4) can be expressed, after some straightforward manipulations, in terms of elliptical integrals,

$$x - x_c = (-\alpha\beta)^{-1/2}\left\{2\left[E\left(\frac{\pi}{2}\middle|m\right) - E(\varphi|m)\right] - \left[F\left(\frac{\pi}{2}\middle|m\right) - F(\varphi|m)\right]\right\}, \qquad (5.7)$$

where $F(\varphi|m)$ and $E(\varphi|m)$ are the elliptical integral of the first and second kind respectively (Abramowitz and Stegun, 1964) with the arguments given by

$$\varphi = \cos^{-1}\left\{\left[\frac{-\alpha\beta}{2(1 - \sin\vartheta_c)}\right]^{1/2}(y - y_c)\right\},$$

$$m = (1 - \sin\vartheta_c)/2.$$

At the turning latitude where (5.5) holds, we have $\varphi = 0$ and hence the quarter-wavelength is given by the expression

$$x - x_c = (-\alpha\beta)^{-1/2}\left[2E\left(\frac{\pi}{2}\middle|m\right) - F\left(\frac{\pi}{2}\middle|m\right)\right]. \qquad (5.8)$$

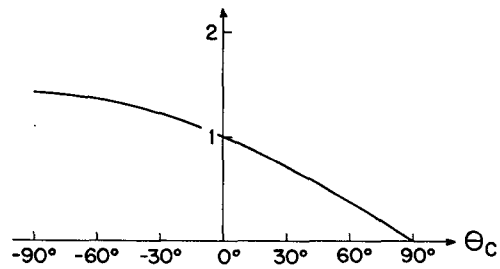

FIG. 10. Figure showing the value of $(-\alpha\beta/2)^{1/2}(y - y_c)$ as a function of ϑ_c.

We have plotted $(-\alpha\beta)^{1/2}(x - x_c)$ in Fig. 11 which is seen to reach a maximum $\pi/2$ when $\vartheta_c = 90°$. Dimensionally, the maximum wavelength thus spans, in terms of the longitudinal degrees,

$$\Delta\Phi \equiv \frac{4(x - x_c)\lambda}{R\cos\Theta_0}$$

$$= \frac{2\pi}{\cos\Theta_0}\left(\frac{\lambda\tan\Theta_0}{-\alpha R}\right)^{1/2} \quad \text{(using Eq. 2.6)}$$

$$= \frac{\pi}{\cos\Theta_0}\Delta\Theta, \quad \text{(using Eq. 5.6)} \qquad (5.9)$$

which is proportional to $\Delta\Theta$ and hence has the same functional dependence on λ and α. It is also noted that the flow loops back on itself at the inflection point when ϑ_c is $-41°$.

6. Other flow characteristics

In Figs. 12 and 13, we have plotted v_L (the velocity at the left boundary of the jet, facing downstream) and the jet width l in the (f, κ) space. For the particular example shown, v_L increases as the current moves along the coast until it separates, after which it becomes constant. Since the jet narrows in the meantime, the current shear increases downstream. Before the separation, the flow curves cyclonically with the coastal boundary and hence reinforces the beta effect in sharpening the anticyclonic current shear. After the separation, however, some of the negative vorticity induced by the beta effect is compensated by the generation of an anticyclonic curvature in the current path and hence, the cross-stream flow structure varies only slowly with a slight narrowing of the jet as it moves poleward. The meandering pattern produced in numerical models (e.g., see Beardsley, 1973) shows some undulation of the jet width, being narrower at the poleward stretches of the meander, presumably due to similar physical mechanisms.

7. Application

Most western boundary currents separate from the coast at one point or another and the model is formulated in a general way so that it can be applied to examine these individual cases. As an example of the model application, we shall however focus on the case of the Agulhas Current which undergoes a dramatic retroflection after separation, the explanation of which is particularly challenging.

For the upstream point, we pick East London at 33°S (with $f_0 \approx -0.79 \times 10^{-4}$) where the coast is relatively straight and where the most recent hydrographic observations are available. One temperature section off East London is shown in Fig. 14 (Gründlingh, 1985) from which we somewhat arbitrarily choose the 10°C isotherm as the model interface so that $H \approx 800$ m, and the reduced gravity g', based on the density dif-

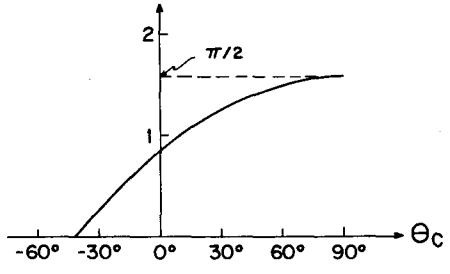

FIG. 11. As in Fig. 10 but for the value of $(-\alpha\beta)^{1/2}(x - x_c)$.

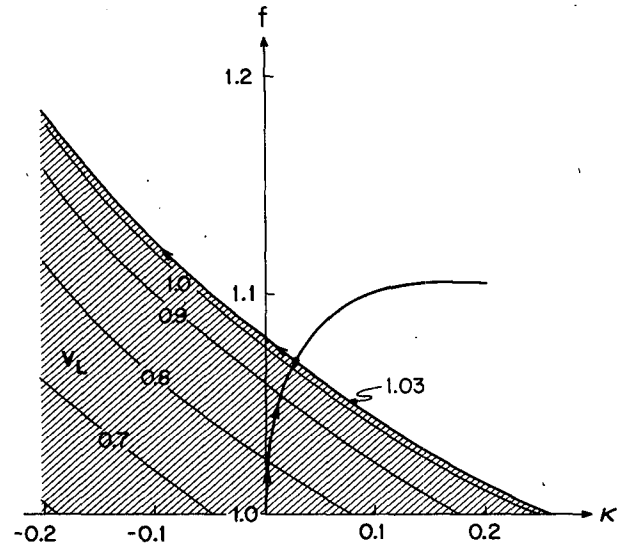

FIG. 12. As in Fig. 5 but for v_L, the velocity at the left boundary of the jet facing downstream.

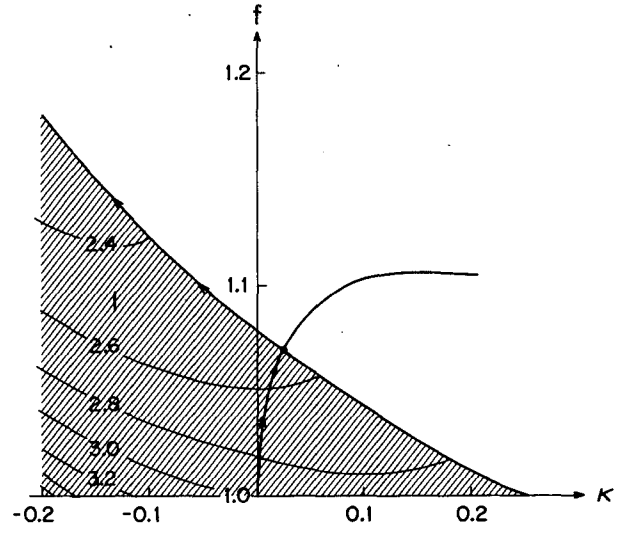

FIG. 13. As in Fig. 5 but for the jet width l.

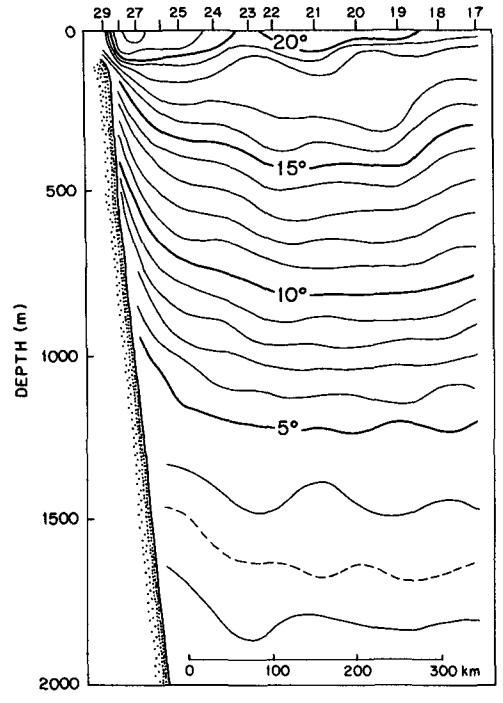

FIG. 14. A temperature section off East London (Gründlingh, 1985).

ference between 5 and 17°C isotherms, is 1.58 cm s^{-2}. Since the primary dimensionless parameter of the model, the volume transport Q, depends only on the interface depth at the coast relative to that offshore of the jet, the model results are not overly sensitive to this particular choice of the 10°C isotherm as the model interface. Based on the above values, the internal radius of deformation is 45 km, the velocity scale is 3.5 m s^{-1}, the volume transport scale is 127×10^6 m^3 s^{-1}, and the dimensionless parameter β has the value 0.011.

Because of the large uncertainty in the observations and the neglect of the frictional effect in the model which must be important near the coast, it is difficult to determine h_{L0} from hydrographic sections. To circumvent this, it is noted however that the inflection point in the current path can be more readily determined from the observations such as that shown in Fig. 1. For this particular observation, the inflection point occurs at about 36°S (hence $f_c \approx 1.08$) and, using the formula (4.2) and (3.1), it implies that $Q \approx 0.46$ and $h_{L0} \approx 0.27$. Dimensionally, the volume transport is thus 59×10^6 m^3 s^{-1}, a reasonable value (Gründlingh, 1980; Gordon, 1985), and the interface depth at coast is 216 m.

With the additional choice of $l_0 = 3$ (or a jet width of about 135 km), the schematic shown in Fig. 5 corresponds to the actual Agulhas Current using above parameter values. The 1000 m isobath has been arbitrarily chosen to represent the coastal boundary and it has been approximated by a smooth line (as shown in Fig. 15). The separation thus occurs at about 35°S, slightly before the inflection point. The slope of the separation curve (α) is −2.53 (see Fig. 7) and, using the formula (5.6), it implies a southernmost turning latitude at 41°S, consistent with observations. The current path calculated from the model is plotted in Fig. 15, which clearly shows the doubling back of the current on itself. Although the model breaks down near the crossing where vigorous mixing must take place, its ability to reproduce the retroflection with roughly the correct dimensions is nevertheless suggestive of its relevance in explaining the phenomenon.

As discussed before, the current path is primarily controlled by the volume transport. In fact, if we decrease the volume transport by 10%, the separation curve does not intersect the coast in Fig. 5, and the current goes around the continent without separation. This possibility was first raised by Veronis (1973) who also conceded that there is no observational evidence that this has ever happened. There is no distinct seasonal cycle in the Agulhas Current transport as reported by Gründlingh (1980, his matched transport). Could it be that (a) the Agulhas Current never weakens sufficiently to go around the African continent, or (b) other dynamical constraints such as that imposed by large scale circulation outside the immediate retroflection area prohibit this occurrence? More study is obviously needed to address the question.

Although no detailed application to other current systems will be attempted here, some further comments might be in order. In the case of the Gulf Stream or Kuroshio, the flow direction at the inflection point lies in the northeast quadrant and, according to Fig. 9, the current meanders after it leaves the coast. The meandering pattern varies greatly and is primarily modulated by the upstream transport. Using realistic parameter values, the maximum amplitude calculated from the model is about 500 km and the maximum wavelength is about 1600 km. It is worth emphasizing that without invoking hydrodynamical instability or topographic steering, a simple model employing only current inertia

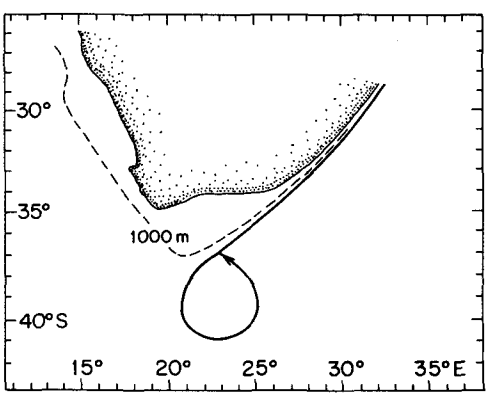

FIG. 15. A calculated path for the Agulhas Current. The dashed line approximates the 1000 m isobath.

and beta effect can produce rather realistic-looking meanders. The model also predicts narrowing (broadening) of the jet as it goes poleward (equatorward). The variation is small, however (less than 10%), and is not likely to be resolved by the existing data. Besides, we might be stretching a simple theory beyond its limit.

8. Discussions

Although highly idealized to isolate certain physical mechanisms and to retain maximum mathematical simplicity, the model, when applied to the Agulhas Current, can reproduce the retroflection feature with roughly the correct dimensions, suggesting that the inertial and beta effect play a dominant role in the phenomenon.

The model, as formulated, also provides a useful framework to examine the effects of some other physical processes neglected in the model. For instance, instead of a free streamline that separates the jet from the ocean interior, the interface depth can be allowed to vary along this streamline. Charney's (1955) solution of the Gulf Stream (his Fig. 1) shows that the interface shallows along the outer streamlines accompanying a downstream increase of the current transport. This shallowing of the interface and the associated velocity increase (due to Bernoulli's law) can be implemented through the boundary conditions and is expected to hasten the separation. The constraints of a vertical coast or a quiescent lower layer may also be relaxed to improve the model applications. The formulation adopted by Gill and Schumann (1979) which couples the two layers to a sloping bottom might be useful in this expansion. Some qualitative effect of the friction may be examined by some parametrical reduction of the potential vorticity or the momentum flux downstream. Although these modifications are believed to be refinements of the present model, they nevertheless may have interesting dynamical consequences and are certainly worthy of further pursuit in the future.

Acknowledgments. We want to thank A. L. Gordon for stimulating our interest in the problem and for providing, along with M. L. Gründlingh, hydrographic data from their recent survey of the Agulhas Current. W. P. M. de Ruijter thanks A. L. Gordon for the opportunity to visit Lamont-Doherty Geological Observatory and the hospitality during the visit. This work is partly supported by the ONR contract N00014-84-C-0132.

APPENDIX A

The Upstream Condition

Setting $f = 1$ and $\rho = \infty$ in (2.4) and (2.7) yields

$$v = \frac{\partial h}{\partial \zeta}, \tag{A1}$$

$$1 + \frac{\partial v}{\partial \zeta} = h. \tag{A2}$$

Multiplying (A1) by h and integrating, we obtain

$$Q = \frac{1}{2}(1 - h_{L0}^2). \tag{A3}$$

(A1) and (A2) can be combined to give

$$\frac{\partial^2 h}{\partial \zeta^2} - h = -1. \tag{A4}$$

Subject to the boundary conditions that

$$\left.\begin{aligned} h &= 1 \quad \text{at} \quad \zeta = l_0 \\ h &= h_{L0} \quad \text{at} \quad \zeta = 0 \end{aligned}\right\},$$

the solution is

$$h = 1 + (1 - h_{L0}) \sinh(\zeta - l_0)/\sinh(l_0). \tag{A5}$$

It follows from (A1) and (A5) that

$$v_R = (1 - h_{L0})/\sinh(l_0).$$

APPENDIX B

The Solution at f_c

Setting $f = f_c$ and $\rho = \infty$ in (2.4) and (2.7) leads to

$$f_c v = \frac{\partial h}{\partial \zeta}, \tag{B1}$$

$$f_c + \frac{\partial v}{\partial \zeta} = h, \tag{B2}$$

which can be combined to give

$$\frac{\partial^2 h}{\partial \zeta^2} - f_c h = -f_c^2. \tag{B3}$$

The general solution of (B3) is

$$h = f_c + A \cosh[\sqrt{f_c}(\zeta - l_c)] + B \sinh[\sqrt{f_c}(\zeta - l_c)]. \tag{B4}$$

where A and B are arbitrary constants and l_c is the jet width yet to be determined.

Using the boundary conditions that

$$h = 1, \quad v = v_R \quad \text{at} \quad \zeta = l_c, \tag{B5}$$

and that

$$h = 0 \quad \text{at} \quad \zeta = 0, \tag{B6}$$

we get

$$A = 1 - f_c,$$

$$B = \sqrt{f_c} v_R,$$

and l_c satisfies the transcendental equation,

$$A \cosh(\sqrt{f_c} l_c) - B \sinh(\sqrt{f_c} l_c) = -f_c.$$

To derive the momentum flux, we first observe that

$$\psi = \int_0^{\zeta} hv d\zeta$$

$$= \frac{1}{2f_c} h^2 \quad \text{(using Eqs. B1 and B6),} \qquad \text{(B7)}$$

hence,

$$M_c \equiv \int_0^{l_c} hv^2 d\zeta$$

$$= \int_0^{l_c} v \frac{\partial \psi}{\partial \zeta} d\zeta \quad \text{(using Eq. 2.1)}$$

$$= [v\psi]_0^{l_c} - \int_0^{l_c} \psi \frac{\partial v}{\partial \zeta} d\zeta \quad \text{(integration by parts)}$$

$$= v_R Q - \frac{1}{2f_c} \int_0^{l_c} h^2 (h - f_c) d\zeta$$

(using Eqs. B2 and B7). (B8)

Substituting (B4) into (B8), we arrive at the expression

$$M_c = v_R Q - \frac{A^2 - B^2}{2} l_c - \frac{\sqrt{f_c} A}{2} (1 + 4Q^2A^2)$$

$$\times \sinh(\sqrt{f_c} l_c) - \frac{\sqrt{f_c} B}{2} (1 - 4Q^2B^2)[1 - \cosh(\sqrt{f_c} l_c)]$$

$$- \frac{A^2 + B^2}{2\sqrt{f_c}} [\sinh(\sqrt{f_c} l_c) \cosh(\sqrt{f_c} l_c)]$$

$$+ \frac{AB}{\sqrt{f_c}} \sinh^2(\sqrt{f_c} l_c) - \frac{QA}{3\sqrt{f_c}} (A^2 + 3B^2) \sinh^3(\sqrt{f_c} l_c)$$

$$- \frac{QB}{3\sqrt{f_c}} (B^2 + 3A^2)[(1 - \cosh^3(\sqrt{f_c} l_c)].$$

REFERENCES

Anderson, D. L. T., and D. W. Moore, 1979: Cross-equatorial inertial jets with special relevance to very remote forcing of the Somali Current. *Deep-Sea Res.*, **26A**, 1–22.

Abramowitz, M., and I. A. Stegun, 1964: *Handbook of Mathematical Functions.* National Bureau of Standards, Washington, DC.

Beardsley, R. C., 1973: A numerical model of the wind-driven ocean circulation in a circular basin. *Geophys. Fluid Dyn.*, **4**, 211–241.

Charney, J. G., 1955: The Gulf Stream as an inertial boundary layer. *Proc. Natl. Acad. Sci. U.S.A.*, **41**, 731–740.

Darbyshire, J., 1972: The effect of bottom topography on the Agulhas Current. *Rev. Pure Appl. Geophys.*, **101**, 208–220.

De Ruijter, W., 1982: Asymptotic analysis of the Agulhas and Brazil Current systems. *J. Phys. Oceanogr.*, **12**, 361–373.

——, and D. Boudra, 1985: The wind-driven circulation in the South Atlantic–Indian Ocean—I. Numerical experiments in a one-layer model. *Deep-Sea Res.*, **32**, 557–574.

Gill, A. E., and E. H. Schumann, 1979: Topographically induced changes in the structure of an inertial coastal jet: Application to the Agulhas Current. *J. Phys. Oceanogr.*, **9**, 975–991.

Gordon, A. L., 1985: Indian-Atlantic transfer of thermocline water at the Agulhas Retroflection. *Science*, **227**, 1030–1033.

——, M. L. Gründlingh and J. R. E. Lutjeharms, 1986: Stratification and circulation of the Agulhas retroflection. In preparation.

Gründlingh, M. L., 1980: On the volume transport of the Agulhas Current. *Deep-Sea Res.*, **27A**, 557–563.

——, 1985: Features of the northern Agulhas Current in spring, 1983. *S. Afr. J. Sci.* (submitted).

Lutjeharms, J. R. E., 1980: Retroflection: When the current turns. *Oceans*, **13**(4), 31.

——, and R. C. van Ballegooyen, 1984: Topographic control in the Agulhas Current system. *Deep-Sea Res.*, **31**(11A), 1321–1337.

Luyten, J. R., 1977: Scales of motion in the deep Gulf Stream and across the Continental Rise. *J. Mar. Res.*, **35**, 49–74.

Moore, D. W., and P. P. Niiler, 1974: A two-layer model for the separation of inertial boundary currents. *J. Mar. Res.*, **32**, 457–484.

Parsons, A. T., 1969: A two-layer model of Gulf Stream separation. *J. Fluid Mech.*, **39**, 511–528.

Richardson, P. L., and J. A. Knauss, 1971: Gulf Stream and Western Boundary Undercurrent observations at Cape Hatteras. *Deep-Sea Res.*, **18**, 1089–1109.

Robinson, A. R., and P. P. Niiler, 1967: The theory of free inertial currents: I. Path and structure. *Tellus*, **19**(2), 269–291.

——, J. R. Luyten and G. Flierl, 1975: On the theory of thin rotating jets: A quasi-geostrophic time dependent model. *Geophys. Fluid Dyn.*, **6**, 211–244.

Røed, L. P., 1980: Curvature effects on hydraulically driven inertial boundary currents. *J. Fluid Mech.*, **96**, 395–412.

Veronis, G., 1973: Model of world ocean circulation: I. Wind-driven, two layer. *J. Mar. Res.*, **31**, 228–288.

Warren, B. A., 1963: Topographic influences on the path of the Gulf Stream. *Tellus*, **15**, 167–183.